The small fiber neuropathy NaV1.7 I228M mutation: impaired neurite integrity *via* bioenergetic and mitotoxic mechanisms, and protection by dexpramipexole

Seong-il Lee[1,2], Janneke G. J. Hoeijmakers[3], Catharina. G. Faber[3], Ingemar. S. J. Merkies[3,4], Giuseppe Lauria[5,6], and Stephen G. Waxman[1,2*]

[1]Department of Neurology, Yale University School of Medicine, New Haven, Connecticut
[2]Center for Neuroscience and Regeneration Research, Veterans Affairs Connecticut Healthcare System, West Haven, Connecticut
[3]Department of Neurology, School of Mental Health and Neuroscience, Maastricht University Medical Center+, Maastricht, the Netherlands
[4]Department of Neurology, St. Elisabeth Hospital, Willemstad, Curaçao
[5]Neuroalgology Unit Foundazione IRCCS Istituto Neurologico, "Carlo Besta" Milan, Italy
[6]Department of Biomedical and Clinical Sciences "Luigi Sacco", University of Milan, Milan, Italy

Corresponding Author*

Email address:
S-IL: **seong.lee@yale.edu**
JGJH: **j.hoeijmakers@mumc.nl**
CGF: **c.faber@mumc.nl**
ISJM: **isjmerkies@hotmail.com**
GL: **Giuseppe.LauriaPinter@istituto-besta.it**
SGW: **stephen.waxman@yale.edu**

Abstract

Gain-of-function variants in voltage-gated sodium channel NaV1.7 that increase firing frequency and spontaneous firing of dorsal root ganglion (DRG) neurons have recently been identified in 5-10% of patients with idiopathic small fiber neuropathy (I-SFN). Our previous *in vitro* observations suggest that enhanced sodium channel activity can contribute to a decrease in length of peripheral sensory axons.

We have hypothesized that sustained sodium influx due to the expression of SFN-associated sodium channel variants may trigger an energetic deficit in neurons which contributes to degeneration and loss of nerve fibers in SFN. Using an ATP FRET biosensor, we now demonstrate reduced steady-state levels of ATP and markedly faster ATP decay in response to membrane depolarization in cultured DRG neurons expressing an SFN-associated variant NaV1.7, I228M, compared to WT neurons. We also observed that I228M neurons show a significant reduction in mitochondrial density and size, indicating dysfunctional mitochondria and a reduced bioenergetic capacity. Finally, we report that exposure to dexpramipexole, a drug that improves mitochondrial energy metabolism, increases the neurite length of I228M-expressing neurons.

Our data suggest that expression of gain-of-function variants of NaV1.7 can damage mitochondria and compromise cellular capacity for ATP production. The resulting bioenergetic crisis can consequently contribute to loss of axons in SFN. We suggest that, besides interventions that reduce ionic disturbance caused by mutant Nav1.7 channels, an alternative therapeutic strategy might target the bioenergetic burden and mitochondrial damage that occur in SFN associated with Nav1.7 gain-of-function mutations.

New and Noteworthy

Sodium channel NaV1.7 mutations that increase dorsal root ganglion (DRG) neuron excitability have been identified in small-fiber neuropathy (SFN). Here we demonstrate reduced steady-state ATP levels, faster depolarization-evoked ATP decay, and reduced mitochondrial density and size in cultured DRG neurons expressing SFN-associated variant NaV1.7-I228M. Dexpramipexole, which improves mitochondrial energy metabolism, has a protective effect. Since gain-of-function Nav1.7 variants can compromise bioenergetics, therapeutic strategies that target bioenergetic burden and mitochondrial damage merit study in SFN.

Introduction

Small fiber neuropathy (SFN) is a painful condition that typically begins to manifest symptoms such as pain and sensory loss in the extremities of the body and spreads to other regions. It is associated with depletion of intraepidermal nerve fiber (IENF)

and damage of unmyelinated and thinly myelinated peripheral nerve fibers in epidermal and dermal layers of the skin. What causes the damage to these sensory nerve fibers and terminals in SFN is not well understood.

Major causes of SFN include *diabetes mellitus*, chemotherapy and viral infection (Kokotis et al. 2016; Polydefkis et al. 2002; Smith et al. 2001). No apparent cause for SFN can be identified in 24% to 93% of cases in published patient series, and these cases are termed idiopathic SFN (I-SFN) (Bednarik et al. 2009; de Greef et al. 2018; Devigili et al. 2008; Lacomis 2002). Recently, Faber *et al.*, demonstrated gain of function (GOF) variants in NaV1.7 in a subset of patients with idiopathic SFN (Faber et al. 2012). Electrophysiological assessment of these variant channels demonstrated that their altered biophysical properties render sensory neurons hyperexcitable, endowing them with a reduced threshold, increased firing frequency, and spontaneous firing of action potentials across a broad range of stimulus intensities, which can contribute to spontaneous pain (Faber et al. 2012; Han et al. 2012a; Han et al. 2012b; Hoeijmakers et al. 2012c). However, little is known about the molecular or cellular bases underlying axonal injury, and IENF depletion in I-SFN associated with GOF variants.

Our previous *in vitro* observations suggest that enhanced sodium channel activity can contribute to a decrease in length of peripheral sensory axons (Persson et al. 2013b). We previously also demonstrated that the activities of normal (wild-type) voltage-gated sodium channels can contribute to growth impairment and degeneration of DRG neurites under metabolically challenging conditions (Persson et al. 2013a). Persistent membrane depolarization and Na^+ influx *via* voltage-gated sodium channels, reverse Na^+/Ca^{++} exchanger, and the consequent ionic disturbance require increased activity of Na^+/K^+ ATPases and Ca^{2+} ATPases to cope with abnormal Na^+ influx and maintain ionic gradient across the membrane (Carafoli 1991; Marunaka 1988).

Mitochondria are a major ATP source in neurons and are essential for the maintenance of nerve fiber integrity (Pellerin et al. 1998; Tantama et al. 2013). Dysfunctional mitochondria have been associated with axonal degeneration in multiple neurodegenerative diseases (Persson et al. 2013a; Takeuchi et al. 2005). Mitochondrial energy metabolism is regulated by several feedback mechanisms to accommodate fluctuating energy demands that reflect dynamic neuronal activities. Increased $[ADP]_i$ and calcium influx induced by neural activity stimulate mitochondrial oxidative phosphorylation (OXPHOS) to compensate the increased ATP consumption (Lark et al. 2016; Rueda et al. 2014). Although OXPHOS constitutes an efficient mechanism to cope with abrupt increase in energy demand in neurons, its excessive activity can negatively impact mitochondrial function and bioenergetics *via* sustained Ca^{2+} influx and ROS generation (Persson et al. 2016).

In this study, we tested the hypothesis that GOF variants in NaV1.7, which are associated with loss of IENFs in I-SFN, may produce a bioenergetic deficit in sensory neurons. To address this question, we employed a cell culture model, and evaluate the effect of an SFN-associated variant NaV1.7, I228M, on neurite length and ATP level in DRG neurons. This particular variant was chosen for study because it previously has been characterized in detail both clinically (Faber et al. 2012) and in terms of its effect on channel and DRG neuron function (Estacion et al. 2011), and because expression of this variant within DRG neurons has a larger effect on neurite integrity *in vitro* than other GOF NaV1.7 mutant channels that have been studied (Persson et al. 2013b). We also examined the effect of the variant channel on mitochondria. Finally, we examined whether a drug that improves mitochondrial energy metabolism protects against the impairment of neurite length in I228M-expressing neurons.

Materials and Methods

Plasmids

The human WT Nav1.7 insert (containing the adult exon 5, E5A, and Long loop1) and the Nav1.7 variant with residue substitutions I228M have been previously described (Estacion et al. 2011). Full-length inserts of clones were sequenced (Howard Hughes Medical Institute/Keck Biotechnology Center at Yale University) and analyzed using BLAST (National Library of Medicine) and Lasergene (DNAStar, Madison, WI).

ATeam1.03-nD/nA/pcDNA(ATeam), the plasmid encoding a FRET-based ATP indicator, has been previously described (Imamura et al. 2009)and was purchased from Addgene (Addgene #51958).

pLV-mito-DsRed, the plasmid encoding a RFP variant tagged with 61 aa targeting sequences of the P1 isoform F1F0-ATP synthase (N terminal on insert) has been previously described (Kitay et al. 2013) and purchased from Addgene (Addgene #44386).

Isolation and culturing of dorsal root ganglion (DRG) neurons

DRG from deeply anesthetized (Ketamine/Xylazine, 80/5 mg/kg bw) C57BL/6 mice (6-8 weeks) were isolated and cultured as described previously (Estacion et al. 2011; Persson et al. 2013a). Briefly, dissected ganglia were placed in ice-cold oxygenated complete saline solution (CSS), containing (in mM) 137 NaCl, 5.3 KCl, 1 $MgCl_2$, 25 sorbitol, 3 $CaCl_2$, 10 *N*-2-hydroxyethylpiperazine-*N*′-2-ethanesulfonic acid (HEPES), pH 7.2, then incubated for 20 minutes in 37°C CSS containing Collagenase A (1.5mg/mL), and for 20 minutes in 37°C CSS containing Collagenase D (1.5 mg/mL) and Papain (30 U/mL). Ganglia were then triturated in DRG media (DMEM/F12

containing 100 U/mL penicillin, 0.1 mg/mL streptomycin (Invitrogen, Carlsbad, CA) and 10% fetal bovine serum (Sigma-Aldrich, St. Louis, MO)), 1.5 mg/mL bovine serum albumin and 1.5 mg/mL trypsin inhibitor (Sigma). The cell pellet was resuspended in DRG media.

Transfection of DRG neurons

The dissociated DRG neurons were transfected by electroporation with WT Nav1.7 channels and Nav1.7 channel variant I228M along with RFP (channel:RFP ratio 10:2), using Nucleofector II (program SCN6; Amaxa, Gaithersburg, MD), as previously described. (Rolyan et al. 2016). WT and I228M neurons were always prepared from the same animal. After isolating the cell suspension, it was split half and half for WT and I228M transfection so that paired cultures, prepared by the same operator on the same day from the same animal, could be compared head-to-head. The transfected neurons were allowed to recover for 5 minutes at 37°C in 0.5 mL of Ca^{2+}-free DMEM. The cell suspension was diluted with Neurobasal A media containing 2% B27, 1% GlutaMax and 100U/ml Penicillin-Streptomycin (Thermo Fisher Scientific) and 150 µL of the cell solution was placed on 15 mm circular poly-L-lysine/laminin-coated coverslips and incubated at 37°C in 5% CO_2 for 30 min. 2ml of the standard culture media (Neurobasal A containing 25mM glucose, 2% B27, 1% GlutaMax and 100U/ml Penicillin-Streptomycin) was added and cells were maintained at 37°C in a 5% CO_2 incubator. For glucose concentration experiments (Figure 2), the standard culture media (25mM glucose) were replaced with 5.7 or 2.7mM glucose- containing Neurobasal A.

Live-cell imaging; neurite outgrowth assay and mitochondrial morphology

Live-cell imaging for neurite measurement was performed using a Nikon Eclipse Ti microscope (Nikon USA, Melville, NY) equipped with an environmental chamber (In Vivo Scientific, St Louis, MO) to maintain the cells in a humidified atmosphere at 37 °C. TRITC filter sets were used to visualize RFP fluorescence, and images were acquired using NIS-Elements (Nikon). For each coverslip, a large-field montage image consisting of 7×7 field-of-view images was acquired using a motorized stage and a 10X objective.

Live-cell imaging for neuritic mitochondria was performed using the same microscope setup. For each condition, 40 images from 2 distinct cultures were acquired using 100X objective and DIC and TRITC filter sets to create two layered images: one including mito-DsRed puncta and one including neurite morphology.

Quantification of neurite lengths

For quantification of neurite lengths, large-field images containing ~50-100 neurons (acquired as described above) were thresholded based on RFP signal using

ImageJ (National Institutes of Health, Bethesda, MS, USA) (with restrictions on signal intensity, size, roundness etc.) to create two binarized layers: one including cell bodies and one including cell bodies as well as neurites. The transfection rate for Schwann cells was very low (<0.01%) and the level of expression of RFP in these cells was low so that these cells were readily excluded by threshold setting. In addition, using roundness setting we were also able to exclude Schwann cells, whose cell bodies are fusiform. Using particle analysis and skeletonize plugins in ImageJ (National Institutes of Health, Bethesda, MS, USA), the total neurite length was calculated for each large-field image and divided by the number of neurons within the field. Thus, a measure of the average neurite length/neuron was acquired for each large-field image. For each condition, 11-34 large-field images were analyzed from 3-8 independent cultures, in each case comparing neurite length/neuron for I228M channel-transfected neurons with neurite length/neuron for WT channel-transfected neurons, cultured at the same time in parallel to insure identical conditions. Normalized data are presented as mean ± SEM where n= number of large-field images, and differences between conditions analyzed using Student's unpaired t-test, and $P<0.05$ was considered significant.

Quantification of mitochondrial morphologies

For quantification of neuritic mitochondrial morphologies, images containing 1 or 2 neurites with mito-DsRed expression (acquired as described above) were thresholded based on DsRed signal using ImageJ. Using particle analysis plugin, total number and size of DsRed puncta were measured from TRITC images. Using line trace and measurement tools in imageJ, total neurite lengths were measured from DIC images. For the mitochondrial density, the total number of DsRed puncta were normalized by total length of neurites within the field. Normalized data are presented as mean ± SEM, differences between conditions analyzed using Student's unpaired t-test, and $P<0.05$ was considered significant.

ATP imaging

Somatic and intraneuritic ATP were assessed using a FRET-based ATP indicator, which increases FRET signal upon binding ATP (Imamura et al. 2009; Pathak et al. 2015). Isolated DRG neurons were transfected with ATeam1.03-nD/nA/pcDNA along with a plasmid encoding either WT or I228M mutant Nav1.7 and cultured in PLL/laminin-treated glass bottom Petri dishes (MatTek). At 4–7 days after plating, FRET images of the cultures were acquired in standard bath solution (SBS) containing the following (in mM): 140 NaCl, 3 KCl, 1 MgCl2, 1 CaCl2, and 10 HEPES, pH 7.3, at room temperature. Neuronal cultures were illuminated with 514-nm light to localize the neurons that were expressing the probe co-transfected with mutant I228M or WT Nav1.7 channels. Neuronal cell bodies identified from YFP signal were

selected for ATP imaging. Neurons with expression of ATP indicator were illuminated with 436 nm using a Nikon Ti-E inverted microscope equipped with a fast switching xenon light source (Lambda DG-4; Sutter Instruments). Dual emission ratio images were captured using a QuantEM CCD camera (Princeton Instruments) and 20X objective (Super Fluor; Nikon) with a DV2 beam splitter (Photometrics) and the following filter sets (Semrock, Rochester, NY); 438/24 - DM458 - 483/32 (CFP) or 542/27 (YFP). The microscope system was controlled with NIS-Elements (Nikon). Imaging data were analyzed using NIS-Elements AR (Nikon). After background correction, YFP/CFP emission ratio was calculated by dividing YFP intensity by CFP intensity for each cell. Normalized data are presented as mean ± SEM, differences between conditions analyzed using Student's unpaired t-test, and $P<0.05$ was considered significant.

Stimulation protocol for ATP imaging

Neuronal culture dishes were microperfused at a constant flow rate using a computerized valve system (ValveLink 8.2; AutoMate Scientific). To measure $[ATP]_i$ transients in activated neuronal cell bodies and neurites, membrane depolarization was induced by perfusion with high $[K^+]$ solution (SBS containing 50 mM KCl/90 mM NaCl). After recording basal level of [ATP] in SBS for 60 s, neurons were exposed to high $[K^+]$ solution. During the microperfusion, neurons were illuminated every 2 s with 492-nm light using a Nikon Ti-E inverted microscope equipped with a fast switching xenon light source (Lambda DG-4; Sutter Instruments). Time lapse Images were captured using a QuantEM CCD camera (Princeton Instruments) and 20 objective(Nikon) under the control of NIS-Elements (Nikon).

The quantification of ATP imaging

Acquired images were digitized and analyzed with NIS-Elements software (Nikon). Based on YFP signal, images were thresholded, and a binary mask created over YFP-positive neuronal cell bodies and neurites. A binary mask overlaying each neuronal cell body was defined as a ROI. For neurites, each 50μm-long segment of the binary mask overlying the neurite was defined as the ROI. Fluorescence at 483-nm (CFP) and 542-nm excitation (YFP) mean pixel intensities were measured. After background correction, the ratio of YFP/CFP was calculated for each image. Mean values from neuronal cell bodies and neurites are depicted in graphs. The area under the curve (AUC) was calculated from t 60 s to t 180 s using Prism8 software (GraphPad). Differences between experimental groups were analyzed by Student's t-test, and $P<0.05$ was considered significant.

Statistics

Statistical analysis was performed using Prism8 software (GraphPad), and either Students' t test or Mann–Whitney rank sum test was used. For neurite data sets, nested t test (Figure 1, 5, and 7), and nested one-way ANOVA (Figure 2) were used to accommodate cluster-related variation. Data are presented as mean ± standard deviation (SD). Mean difference ± SEM (MD) and 95% confidence intervals (CI) were also calculated to assess the magnitude of these differences. Statistical significance was accepted at $p \leq 0.05$ for all variables.

Effect size estimates for ATP FRET

FRET in Figure 3 is an arbitrary measurement for ATP levels. For more objective comparison of treatment effects in figure 3B and 3D, we standardized the effect sizes, using Cohen's d effect sizes (ES) with the resulting d values reported (Cohen 1988; Lenhard et al. 2016). We used an effect size calculator that considers standard deviation and sample number variation between groups as well as their non-parametric distributions (Lenhard et al. 2016; Fritz et al. 2012).

In this calculation, Cohen's d is computed from the equation;

$$d = \frac{2r}{\sqrt{1 - r^2}}$$

, where the point biserial correlation r is derived from U values from Mann-Whitney tests and sample sizes n of two groups, using Hans Wendt formula (Wendt, 1972),

$$r = \frac{1 - (2U)}{n_1 \times n_2}$$

Availability of data and materials

The datasets that support the findings of this study have been deposited in figshare at https://figshare.com/s/5f02c47d446893384c34.

Results

I228M, an SFN-associated Nav1.7 gain of function mutant, reduces the neurite length of cultured DRG neurons

Loss of intraepidermal nerve fibers (IENFs) is a hallmark of SFN and an important diagnostic criterion of the disease. We previously reported that GOF mutations in NaV1.7 are associated with I-SFN and showed that expression of these mutations renders sensory neurons hyperexcitable. In addition, following the expression of the GOF variants, dorsal root ganglion (DRG) neurons exhibit reduced nerite lengths (Persson et al. 2013b; Rolyan et al. 2016).

To establish an *in vitro* model for IENF loss by SFN-associated GOF variants in NaV1.7, we transfected DRG neurons with wild-type (WT) and variant I228M

NaV1.7 channels (co-transfected with red fluorescent protein [RFP] to enable the identification of transfected cells). As demonstrated in representative 49 field-of-view montage images (Figure 1A and C), cultures contained numerous RFP-positive neurons, 7 days after transfection, with robust RFP signal in cell bodies as well as neurites. Cell diameters varied between 20**μ**m and 60**μ**m. Examples of neurons transfected with WT and I228M are shown at increased magnification in Figure 1B and D.

Mean total neurite length/neuron was quantified from large-field images for WT- and I228M-transfected neurons. There was an 20% reduction ($p < 0.0001$) in length of neurites of I228M-expressing neurons as compared to those transfected with WT channels (Figure 1E). We did not differentiate between large and small diameter DRG neurons because neurites from each neuron made multiple crossings with neurites from adjacent neurons, making it impossible to locate the cell body (or cell body diameter) from which any given neurite arose.

DRG neurons expressing I228M exhibit decreased neurite length in low glucose concentration.

Neurite growth and/or the maintenance of neurite length *via* extension and regeneration is a high-energy demanding cellular process. Metabolically challenging conditions, especially associated with the shortage of ATP, prevent neurite extension and induce neurite degeneration (Chen et al. 2007; Estacion et al. 2015; Persson et al. 2016).

Glucose is a major substrate for ATP production and its availability affects cellular energetics (Tanaka et al. 2014; Tanaka et al. 2015; Tantama et al. 2013). We therefore examined how low glucose availability would affect neurite growth of cultured neurons. WT channel-expressing neurons exhibited similar neurite lengths in all three glucose concentrations (25, 5.7 and 2.7mM) with a trend of modestly increased neurite length in lower concentrations (Figure 2A). This result suggests that, in neurons that express normal (wild-type) voltage-gated sodium channels, neurite lengths are not strongly dependent on glucose availability in this model system, presumably because the channel activity and the resulting cellular activities are not a burden on neuronal bioenergetics.

In contrast to the WT cells, I228M neurons showed a trend toward markedly decreased neurite lengths at low glucose concentrations (5.7 and 2.7mM), compared to those in the control glucose condition (25mM) (Figure 2B). Average neurite length was reduced by 25% (*p=0.015*) in 2.5mM glucose, as compared to the control. Our results indicate that the presence of I228M channels imposes energetic burden on sensory fibers, rendering them more vulnerable to damage under conditions where the glucose level is low.

DRG neurons expressing I228M exhibit a reduced steady-state level of ATP

Impaired slow-inactivation of I228M is known to produce a sustained influx of sodium, which would be predicted to lead to persistent activation of Na^+/K^+ ATPase pumps (Estacion et al. 2015). The presence of I228M also produces increased spontaneous firing of DRG neurons (Estacion et al. 2011). The firing of action potentials induces synaptic vesicle cycling that imposes an additional energetic cost (Pathak et al. 2015). We therefore expected that I228M-transfected neuron would display low intracellular ATP level ($[ATP]_i$).

To address this question, we measured ATP levels in DRG neurons using a genetically encoded FRET sensor, Ateam (Imamura et al. 2009). We transfected DRG neurons with NaV1.7 wild type (WT) or I228M along with Ateam FRET sensor and measured FRET (ratio between YFP emission/ CFP emission) signals from the transfected cells 5-6 days after culturing. We compared FRET differences between WT and I228M groups.

It is not clear if the relationship of FRET values and ATP levels is linear. Recognizing this limitation, inferential statistical analysis was carried out using Cohen's d effect sizes (Cohen 1988), which allows us to achieve standardized comparison of treatment effect by NaV1.7 I228M (small effect = 0.20, medium effect = 0.50 and large effect = 0.80). We calculated the effect sizes in the results of Figure 3, using an effect size calculator that considers standard deviation and sample number variation between groups as well as their non-parametric distributions (Lenhard et al. 2016).

As shown in Figure 3A and B, I228M neurons displayed a modest reduction in the FRET signal, compared to that of WT. Our test statistic (p = 0.0042) signifies this reduction in the I228M. However, given the small effect size (Cohen's d = 0.315, whether or not the effect size of this result is biologically meaningful remains to be determined under the conditions that might permit changes of larger magnitude in ATP level to occur.

Several feedback mechanisms might participate in the regulation of mitochondrial ATP synthesis in these neurons. A moderate ATP reduction in I228M neurons (Figure 3B) might be explained as a result of increased mitochondrial metabolisms *via* feedback regulations (Estacion et al. 2015; Rolyan et al. 2016). We therefore treated both WT and I228M DRG cultures with 1μM rotenone to inhibit mitochondrial function and compared their steady-state levels of ATP. Rotenone markedly reduced the FRET level in both WT and I228M cultures, indicating a significant mitochondrial contribution to the FRET signal (Figure 3B and D). However, in the presence of rotenone, I228M-transfected neurons showed a more robust decrease in their FRET signal, compared to WT neurons. The average FRET value of WT neurons shifted from 3.738 to 3.408 (9% reduction, Cohen's d = 0.315) whereas the FRET signal in I228M cultures shifted from 3.542 to 3.031 (15%

reduction, Cohen's d = 0.364) (Figure 3B and D). This result suggests that I228M channels negatively impact neuronal bioenergetics *via* a reduction in $[ATP]_i$, for which mitochondria can partially compensate.

DRG neurons expressing I228M exhibit a faster decay of $[ATP]_i$ in response to membrane depolarization

DRG neurons expressing I228M channels display an increased firing frequency over a broad range of stimulus intensities even close to current threshold (Estacion et al. 2011). We therefore asked how I228M expression influences the change of $[ATP]_i$ in response to depolarization. We induced membrane depolarization in the transfected DRG neurons *via* application of 50mM KCl and monitored the FRET change of the ATP sensor in real-time.

As shown in figure 4, both WT- and I228M-transfected neurons displayed a decrease in the FRET signal of ATeam in both cell bodies and neurites in response to high K^+ application. However, the magnitude of the FRET reduction was greater in I228M neurons than in WT neurons, suggesting that I228M neurons deplete their $[ATP]_i$ more rapidly than that of WT. More rapid reductions of the FRET signal were demonstrated in neurites than cell bodies (Figure 4B and D), possibly due to the smaller diameter of neurites which are known to express a high level of sodium channels (Black et al. 2012; Persson et al. 2010). Irrespective of the underlying biophysical mechanism, the results indicate that neurites expressing I228M channels are bioenergetically more vulnerable to energetic stress imposed by depolarization than cell bodies, and that this vulnerability is markedly enhanced under the expression of I228M channels.

Pyruvate moderately increases neurite length in I228M neurons

Cellular ATP is produced in part from the activities of glycolysis and mitochondrial OXPHOS. Greater molar numbers of ATP are synthesized from OXPHOS, utilizing pyruvate as a substrate (Figure 5A). Increasing pyruvate availability has been demonstrated to facilitate mitochondrial ATP production and prevent cell and tissue damage provoked by conditions that involve bioenergetic stress (Geng et al. 2015; Izumi and Zorumski 2010; Peeling et al. 1996; So and Fuller 2003; Wang et al. 2018; Zeng et al. 2007).

We hypothesized that exogenous pyruvate might protect against the impairment of neurite outgrowth in I228M-transfected neurons. To test this hypothesis, we cultured I228M-expressing DRG neurons for 7 days in the absence and presence of pyruvate and compared the neurite lengths under these conditions. In contrast to this expectation, pyruvate treatment failed to significantly increase neurite length in I228M neurons, despite a trend of slight increase (Figure 5B, left panel).

We initially reasoned that this result might reflect negative feedback regulation from glycolysis that would inactivate pyruvate dehydrogenase (Figure 5A). Because high glucose concentration in the culture condition is expected to strengthen the inhibition of pyruvate dehydrogenase (PDH) through PDH kinase (PDK) phosphorylation and prevent pyruvate from being incorporated into OXPHOS, we used dichloroacetate (DCA), a PKD inhibitor, to increase pyruvate flux into mitochondrial metabolism and evaluated its effect on neurite length of I228M neurons. However, DCA treatment was also ineffective in promoting neurite length of I228M neurons (Figure 5B, right panel).

I228M neurons display a marked reduction in the size and number of mitochondria.

We reasoned that the failure of the previous metabolic approaches might reflect alterations of mitochondria in I228M neurons. To address this possibility, we investigated the size and density of mitochondria, which are strongly associated with the functionality and bioenergetic capacity of the organelles (Youle and van der Bliek 2012). We transfected DRG neurons with Mito-dsRED whose fluorescence is limited to mitochondria and assessed their morphologies and distribution in the transfected neurons. As shown in Figure 6, red fluorescence was expressed as puncta along the neurites, confirming the target specificity of Mito-DsRed (Kitay et al. 2013). In a comparison of WT and I228M cultures (Figure 6), I228M-expressing neurites exhibited significantly fewer DsRed puncta than WT-expressing ones. In addition, the size of DsRed puncta in I228M-neurites was significantly diminished, compared to that of WT neurites.

The extent of mitochondrial fusion and fission provide indices of the intactness of the subcellular organelle. Fragmented mitochondria, indicating increased fission, are in general associated with mitochondrial damage and reduced respiratory capacity (Rossignol et al. 2004; Westermann 2012). These results thus suggest that I228M expression leads to dysfunctional and degrading mitochondria, which is consistent with the ineffectiveness of pyruvate and DCA treatment in neurite length enhancement. They also suggest that mitochondrial alterations are at least in part involved in the reduced cellular energy state and neurite length in the mutant cells.

Dexpramipexole increases neurite length in I228M neurons.

Our results — short neurite length, impaired bioenergetics, and mitochondrial alterations in I228M neurons — predict that agents that protect or restore mitochondrial energy production might protect against the impairment of neurite length by GOF variants in NaV1.7.

An electrochemical gradient of protons is created by cellular respiratory activities of mitochondria. The ionic gradient across the inner mitochondrial

membrane is used to drive ATP synthesis. Maintaining the gradient is, therefore, critical to ensure sufficient ATP production *via* mitochondrial OXPHOS.

The mitochondrial permeability transition pore (mPTP) is known to regulate the ionic gradient in mitochondrial matrix. Despite its role in the regulation of mitochondrial Ca^{2+} level and metabolism, pathological conditions related to energetic stress and Ca^{2+} overload can cause prolonged opening of mPTP, and in turn induce mitochondrial dysfunction.

Dexpramipexole (DEX) blocks mPTP, enhances mitochondrial membrane potential and improves mitochondrial energy metabolism in models of neurodegeneration (Alavian et al. 2015; Alavian et al. 2012). To determine whether DEX protects against reduced neurite length of I228M neurons, we treated the neurons with this drug at a concentration previously reported to increase ATP levels in neuronal cultures (Alavian et al. 2012). As shown in Figure 7E, treated neurons displayed a significant increase in neurite length, compared to untreated group in parallel cultures. Mean total length/neuron was increased by 25% in DEX-treated I228M neurons. We also assessed the effect of DEX on WT neurons and found that 2μM DEX did not alter neurite length of WT-transfected neurons (Figure 7F).

Those results indicate that mitochondrial mechanisms are indeed involved in the neuritic impairment of I228M neurons. They also suggest that a therapeutic strategy might target mitochondrial dysfunction to prevent IENF loss that occurs in DRG neurons carrying GOF mutations in NaV1.7.

Discussion

Gain-of-function mutations in NaV1.7 are related to loss of intraepidermal nerve fibers in I-SFN and reduce neurite lengths in cultured DRG neurons

The epidermis where IENFs reside is a dynamic terrain. The tissue continuously remodels itself. Because new keratinocytes arise at the base of the tissue, then migrate upwards and flatten preexisting keratinocytes, there is an ongoing change of intercellular space and extracellular matrix, which mandates IENFs to navigate through and adjust their ramification patterns while maintaining their skin innervation. IENFs achieve this goal by a dynamic process that involves repeated regeneration and degeneration (Cheng et al. 2010; Gibbons et al. 2010; Verze et al. 1999).

Previous skin biopsy studies have revealed that the density of nerve fibers innervating the epidermis is reduced, and some nerve fiber terminals display degenerating or retracting morphologies in the epidermis of SFN patients harboring GOF mutations in NaV1.7. Those observations suggest that the sensory nerve fibers

in SFN are "dying back" (Chai et al. 2005; Hoeijmakers et al. 2012b; Lauria et al. 2011).

The neurite outgrowth assay provides a simple *in vitro* method for assessment of potential effects of genetic and exogenous factors on the integrity of the axons of DRG neurons. (Filous and Silver 2016). In the present study, we chose the I228M mutation of NaV1.7 because it has been characterized in detail both clinically (Faber et al. 2012) and in terms of its effect on channel and DRG neuron function (Estacion et al. 2011), and because expression of this variant within DRG neurons has a larger effect on neurite integrity *in vitro* than other gain-of-function NaV1.7 mutant channels that have been studied (Persson et al. 2013b). Using this *in vitro* assay, DRG neurons transfected with I228M showed a reduced neurite length, compared to WT channels (Figure 1).

Gain-of-function mutations in NaV1.7 produce a bioenergetic deficit.

Despite the statistical significance of our results in Figure 3, their small effect sizes approximately equate to a 58.4-61.1% probability of superiority, suggesting that the effect of I228M in this condition might be minimal at best (calculated from https://rpsychologist.com/d3/cohend/). Whether or not a 0.3-0.4 standard deviation difference between groups is biologically relevant remains to be determined through further investigation. In SFN patients, neurodegeneration occurs in length-dependent and age-dependent manners (Hoeijmakers et al. 2012a). Given this clinical feature of SFN, culturing for longer periods of time, under conditions that permit growth of longer axons and cumulative ATP reduction or mitotoxic effect, might permit changes of larger magnitude in ATP level to occur.

I228M-expressing neurons demonstrated reduced levels of $[ATP]_i$ in the basal state and increased ATP consumption rates in response to depolarization (Figure 3 and 4). These results suggest that decreased bioenergetic stores contribute to the pathophysiology of SFN related to GOF variants of NaV1.7. Those mutations alter the gating properties of the channels so that their pores open more frequently and/or with longer duration(Estacion et al. 2011; Hoeijmakers et al. 2012c). Those alterations expectedly increase Na^+ influx and, *via* reverse operation of Na^+/Ca^{++} exchanger, alter $[Ca^{2+}]_i$ dynamics in neurons as demonstrated by the example of G856D mutation (Estacion et al. 2015). To reverse the resulting ionic imbalance, the excessive Na^+ and Ca^{2+} are necessarily pumped out, which requires increasing activities of Na^+/K^+-ATPase and Ca^{2+}-ATPase (Ames et al. 1992; Palmgren and Nissen 2011; Sokoloff 1999). The increased activities of these pumps can impose an energetic burden to neurons. In addition to that ionic disturbance, the variant channels render neurons hyperexcitable with higher firing frequency and increased spontaneous firing of action potentials that can confer an additional energetic burden. (Estacion et al. 2011; Han et al. 2012a; Han et al. 2012b; Hoeijmakers et al. 2012a).

Cellular energy state influences neurite length

Multiple studies have suggested a link between bioenergetic state and the maintenance of axonal integrity (Chowdhury et al. 2014; Estacion et al. 2015; Persson et al. 2013a). Numerous cellular events take part in axon extension and maintenance, including actin-microtubule reorganization, vesicle trafficking and protein synthesis, and some of them are energetically demanding. It is thus not surprising that impaired bioenergetic states have been shown to result in axonal injury, growth inhibition and degeneration *in vitro* (Gibbons et al. 2010; Kitayama et al. 2008; Natera-Naranjo et al. 2012; Persson et al. 2013a; Press and Milbrandt 2008). The continuous remodeling, that is required for IENFs *in vivo* to maintain skin innervation as they accommodate to the addition of new epidermal cells and their transit to the skin surface, may add to the energetic demand.

Our results suggest that a bioenergetic deficit contributes to the mechanism by which GOF variants in NaV1.7 cause IENF loss. First, under the expression of I228M mutant channels, DRG neurons displayed reduced steady-state levels of $[ATP]_i$ and rapid ATP consumption rates upon membrane depolarization. This result indicates that the mutant channels impose bioenergetic stress on sensory neurons and their nerve fibers. Second, neurite lengths in I228M neurons were markedly sensitive to glucose availability, while this effect was not observed in WT cells. This result suggests that the energetic burden by GOF variants in NaV1.7 renders nerve fibers vulnerable to metabolic conditions that are benign to WT axons. Given that the low glucose concentrations that we used fall within physiological ranges (Guemes et al. 2016), we suggest that the GOF variant channels trigger axonal damage at least in part *via* a bioenergetic mechanism in I-SFN.

Mitotoxicity and protection in peripheral sensory neuropathies

The alterations of mitochondria in I228M neurons (Figure 6) indicate that mitochondrial mechanisms also contribute to impaired bioenergetics and IENF damage in I-SFN related to NaV1.7 mutations. Dysfunction and/or loss of mitochondria have been recently suggested as a converging pathogenic mechanism in multiple types of peripheral neuropathy (Bennett et al. 2014; Casanova-Molla et al. 2012; Lehmann et al. 2011; Persson et al. 2016). DEX has been shown to have a protective effect in several models of neurodegeneration (Alavian et al. 2015; Alavian et al. 2012). The beneficial effect of DEX in our model system (Figure 7) suggests the possibility that at least in the short term, a degree of therapeutic protection of IENF may be achievable.

Bioenergetic stress and pain

Bioenergetic stress impairs the performance of Na^+-K^+-ATPase-dependent pump. This impairment contributes to a depolarizing shift in resting membrane potential, which can render neurons hyperexcitable prior to development of neuropathy (Nasu et al. 2014). Ischemic conditions are also known to result in bioenergetic deficits and increase membrane depolarization and axonal excitability (Han et al. 2008; Kiernan and Bostock 2000). Those results are consistent with our hypothesis and observations — GOF variants in NaV1.7 evoke bioenergetic stress, resulting in the impairment of the ATPases pumps and a disturbance of ionic gradient. We suggest that the ionic disturbance evoked by the variant channels and the consequent energetic burden may mutually amplify each other. The resulting positive feedback loop may, in the long term, aggravate spontaneous impulse generation and pain in SFN. For instance, increased ionic perturbation would decrease cellular energy. This energy crisis would consequently impair the function of the ATPase-dependent ion pumps. As a result, the residual ionic imbalance would be expected to persistently activate ATPases, further depriving cellular ATP. Through this cycling between ionic imbalance and bioenergetic stress, neurons would be increasingly depolarized and deprived of cellular energy. If affected neurons are nociceptors, this would contribute to an increased spontaneous pain. If such a cycling persists, the consequent severe bioenergetic crisis would lead to neurodegeneration of IENF.

Multiple GOF mutations of NaV1.7 have been linked to small fiber neuropathy (Faber et al. 2012; Han et al. 2012a; Han et al. 2012b). In previous studies, a subset of DRG neurons expressing the SFN G856D mutation demonstrated time-dependent neurite degeneration as well as neurite fragmentation under metabolically challenging conditions (Estacion et al. 2015; Rolyan et al. 2016). However, the G856D mutation produces a complex phenotype in which impaired distal limb development accompanies SFN (Hoeijmakers et al. 2012c). We speculate that many gain-of-function NaV1.7 mutations impose energetic stress on DRG neurons. Additional studies on other NaV1.7 mutant channels will be needed to confirm this proposal. Additional studies will be needed to determine whether bioenergetic or mitotoxic mechanisms contribute to the association that has been reported (Blesneac et al. 2018) between NaV1.7 mutations and painful diabetic neuropathy.

Conclusion

SFN is a progressive disorder and is often diagnosed when there is degeneration of nerve fibers. Our result suggests that, in addition to interventions that selectively reduce ionic imbalances caused by mutant Nav1.7 channels, an alternative therapeutic strategy might target the bioenergetic burden and mitochondrial dysfunction that occur in SFN associated with Nav1.7 gain-of-function mutations. Future studies will be needed to assess this approach with multiple SFN-associated

sodium channel mutations, and should aim at testing this mechanism *in vivo*, *via* the assessment of IENF and behavioral changes after interventions that protect bioenergetic mechanisms.

Acknowledgements

We thank Peng Zhao and Lawrence Macala for superb technical assistance and Monique M. Gerrits and Daria Sizova for helpful suggestions.

Competing interests

Dr. Faber reports grants from European Union's Horizon 2020 research and innovation programme Marie Sklodowska-Curie grant for PAIN-Net, Molecule-to-man pain network (grant no. 721841), grants from Prinses Beatrix Spierfonds, grants from Grifols and Lamepro for a trial on IVIg in small fibre neuropathy, other from Steering committtees/advisory board for studies in small fibre neuropathy of Biogen/Convergence and Vertex, outside the submitted work.

Dr. Merkies reports Participation in steering committees of the Talecris ICE Study, CSL Behring, LFB, Novartis, Octapharma, Biotest and UCB, grants from Grifols and Lamepro for a trial on IVIg in small fibre neuropathy, outside the submitted work.

Dr. Hoeijmakers reports a grant from Prinses Beatrix Spierfonds, outside the submitted work. Dr. Waxman reports serving as an advisor or consultant to Amgen, Biogen, GlaxoSmithKline, Chromocell, and SiteOne Therapeutics.

References

Alavian KN, Dworetzky SI, Bonanni L, Zhang P, Sacchetti S, Li H, Signore AP, Smith PJ, Gribkoff VK, and Jonas EA. The mitochondrial complex V-associated large-conductance inner membrane current is regulated by cyclosporine and dexpramipexole. *Mol Pharmacol* 87: 1-8, 2015.

Alavian KN, Dworetzky SI, Bonanni L, Zhang P, Sacchetti S, Mariggio MA, Onofrj M, Thomas A, Li H, Mangold JE, Signore AP, Demarco U, Demady DR, Nabili P, Lazrove E, Smith PJ, Gribkoff VK, and Jonas EA. Effects of dexpramipexole on brain mitochondrial conductances and cellular bioenergetic efficiency. *Brain Res* 1446: 1-11, 2012.

Ames A, 3rd, Li YY, Heher EC, and Kimble CR. Energy metabolism of rabbit retina as related to function: high cost of Na+ transport. *J Neurosci* 12: 840-853, 1992.

Bednarik J, Vlckova-Moravcova E, Bursova S, Belobradkova J, Dusek L, and Sommer C. Etiology of small-fiber neuropathy. *J Peripher Nerv Syst* 14: 177-183, 2009.

Bennett GJ, Doyle T, and Salvemini D. Mitotoxicity in distal symmetrical sensory peripheral neuropathies. *Nat Rev Neurol* 10: 326-336, 2014.

Black JA, Frezel N, Dib-Hajj SD, and Waxman SG. Expression of Nav1.7 in DRG neurons extends from peripheral terminals in the skin to central preterminal branches and terminals in the dorsal horn. *Mol Pain* 8: 82, 2012.

Blesneac I, Themistocleous AC, Fratter C, Conrad LJ, Ramirez JD, Cox JJ, Tesfaye S, Shillo PR, Rice ASC, Tucker SJ, and Bennett DLH. Rare NaV1.7 variants associated with painful diabetic peripheral neuropathy. *Pain* 159: 469-480, 2018.
Carafoli E. Calcium pump of the plasma membrane. *Physiol Rev* 71: 129-153, 1991.
Casanova-Molla J, Morales M, Garrabou G, Sola-Valls N, Soriano A, Calvo M, Grau JM, and Valls-Sole J. Mitochondrial loss indicates early axonal damage in small fiber neuropathies. *J Peripher Nerv Syst* 17: 147-157, 2012.
Chai J, Herrmann DN, Stanton M, Barbano RL, and Logigian EL. Painful small-fiber neuropathy in Sjogren syndrome. *Neurology* 65: 925-927, 2005.
Chen W, Mi R, Haughey N, Oz M, and Hoke A. Immortalization and characterization of a nociceptive dorsal root ganglion sensory neuronal line. *J Peripher Nerv Syst* 12: 121-130, 2007.
Cheng C, Guo GF, Martinez JA, Singh V, and Zochodne DW. Dynamic plasticity of axons within a cutaneous milieu. *J Neurosci* 30: 14735-14744, 2010.
Chowdhury SR, Saleh A, Akude E, Smith DR, Morrow D, Tessler L, Calcutt NA, and Fernyhough P. Ciliary Neurotrophic Factor Reverses Aberrant Mitochondrial Bioenergetics Through the JAK/STAT Pathway in Cultured Sensory Neurons Derived from Streptozotocin-Induced Diabetic Rodents. *Cellular and Molecular Neurobiology* 34: 643-649, 2014.
Cohen J . Statistical Power Analysis for the Behavioral Sciences. 1988
de Greef BTA, Hoeijmakers JGJ, Gorissen-Brouwers CML, Geerts M, Faber CG, and Merkies ISJ. Associated conditions in small fiber neuropathy - a large cohort study and review of the literature. *Eur J Neurol* 25: 348-355, 2018.
Devigili G, Tugnoli V, Penza P, Camozzi F, Lombardi R, Melli G, Broglio L, Granieri E, and Lauria G. The diagnostic criteria for small fibre neuropathy: from symptoms to neuropathology. *Brain* 131: 1912-1925, 2008.
Estacion M, Han C, Choi JS, Hoeijmakers JG, Lauria G, Drenth JP, Gerrits MM, Dib-Hajj SD, Faber CG, Merkies IS, and Waxman SG. Intra- and interfamily phenotypic diversity in pain syndromes associated with a gain-of-function variant of NaV1.7. *Mol Pain* 7: 92, 2011.
Estacion M, Vohra BP, Liu S, Hoeijmakers J, Faber CG, Merkies IS, Lauria G, Black JA, and Waxman SG. Ca2+ toxicity due to reverse Na+/Ca2+ exchange contributes to degeneration of neurites of DRG neurons induced by a neuropathy-associated Nav1.7 mutation. *J Neurophysiol* 114: 1554-1564, 2015.
Faber CG, Hoeijmakers JG, Ahn HS, Cheng X, Han C, Choi JS, Estacion M, Lauria G, Vanhoutte EK, Gerrits MM, Dib-Hajj S, Drenth JP, Waxman SG, and Merkies IS. Gain of function Nanu1.7 mutations in idiopathic small fiber neuropathy. *Annals of neurology* 71: 26-39, 2012.
Filous AR, and Silver J. Neurite Outgrowth Assay. *Bio Protoc* 6: 2016.
Fritz CO, Morris PE and Richler JJ. Effect Size Estimates: Current Use, Calculations, and Interpretation Journal of Experimental Psychology; General. 141: 2-18, 2012.
Geng X, Elmadhoun O, Peng C, Ji X, Hafeez A, Liu Z, Du H, Rafols JA, and Ding Y. Ethanol and normobaric oxygen: novel approach in modulating pyruvate dehydrogenase complex after severe transient and permanent ischemic stroke. *Stroke* 46: 492-499, 2015.
Gibbons CH, Wang N, and Freeman R. Capsaicin induces degeneration of cutaneous autonomic nerve fibers. *Annals of neurology* 68: 888-898, 2010.
Guemes M, Rahman SA, and Hussain K. What is a normal blood glucose? *Arch Dis Child* 101: 569-574, 2016.
Han C, Hoeijmakers JG, Ahn HS, Zhao P, Shah P, Lauria G, Gerrits MM, te Morsche RH, Dib-Hajj SD, Drenth JP, Faber CG, Merkies IS, and Waxman SG. Nav1.7-related small

fiber neuropathy: impaired slow-inactivation and DRG neuron hyperexcitability. *Neurology* 78: 1635-1643, 2012a.
Han C, Hoeijmakers JG, Liu S, Gerrits MM, te Morsche RH, Lauria G, Dib-Hajj SD, Drenth JP, Faber CG, Merkies IS, and Waxman SG. Functional profiles of SCN9A variants in dorsal root ganglion neurons and superior cervical ganglion neurons correlate with autonomic symptoms in small fibre neuropathy. *Brain* 135: 2613-2628, 2012b.
Han SE, Boland RA, Krishnan AV, Vucic S, Lin CS, and Kiernan MC. Changes in human sensory axonal excitability induced by an ischaemic insult. *Clin Neurophysiol* 119: 2054-2063, 2008.
Hoeijmakers JG, Faber CG, Lauria G, Merkies IS, and Waxman SG. Small-fibre neuropathies--advances in diagnosis, pathophysiology and management. *Nat Rev Neurol* 8: 369-379, 2012a.
Hoeijmakers JG, Faber CG, Lauria G, Merkies IS, and Waxman SG. Small-fibre neuropathies—advances in diagnosis, pathophysiology and management. *Nature Reviews Neurology* 8: 369, 2012b.
Hoeijmakers JG, Han C, Merkies IS, Macala LJ, Lauria G, Gerrits MM, Dib-Hajj SD, Faber CG, and Waxman SG. Small nerve fibres, small hands and small feet: a new syndrome of pain, dysautonomia and acromesomelia in a kindred with a novel NaV1.7 mutation. *Brain* 135: 345-358, 2012c.
Imamura H, Nhat KP, Togawa H, Saito K, Iino R, Kato-Yamada Y, Nagai T, and Noji H. Visualization of ATP levels inside single living cells with fluorescence resonance energy transfer-based genetically encoded indicators. *Proc Natl Acad Sci U S A* 106: 15651-15656, 2009.
Izumi Y, and Zorumski CF. Neuroprotective effects of pyruvate following NMDA-mediated excitotoxic insults in hippocampal slices. *Neurosci Lett* 478: 131-135, 2010.
Kiernan MC, and Bostock H. Effects of membrane polarization and ischaemia on the excitability properties of human motor axons. *Brain* 123 Pt 12: 2542-2551, 2000.
Kitay BM, McCormack R, Wang Y, Tsoulfas P, and Zhai RG. Mislocalization of neuronal mitochondria reveals regulation of Wallerian degeneration and NMNAT/WLD(S)-mediated axon protection independent of axonal mitochondria. *Hum Mol Genet* 22: 1601-1614, 2013.
Kitayama H, Miura Y, Ando Y, Hoshino S, Ishizaka Y, and Koyanagi Y. Human Immunodeficiency Virus Type 1 Vpr Inhibits Axonal Outgrowth through Induction of Mitochondrial Dysfunction. *Journal of Virology* 82: 2528, 2008.
Kokotis P, Schmelz M, Kostouros E, Karandreas N, and Dimopoulos MA. Oxaliplatin-Induced Neuropathy: A Long-Term Clinical and Neurophysiologic Follow-Up Study. *Clin Colorectal Cancer* 15: e133-140, 2016.
Lacomis D. Small-fiber neuropathy. *Muscle Nerve* 26: 173-188, 2002.
Lark DS, Torres MJ, Lin CT, Ryan TE, Anderson EJ, and Neufer PD. Direct real-time quantification of mitochondrial oxidative phosphorylation efficiency in permeabilized skeletal muscle myofibers. *Am J Physiol Cell Physiol* 311: C239-245, 2016.
Lauria G, Cazzato D, Porretta-Serapiglia C, Casanova-Molla J, Taiana M, Penza P, Lombardi R, Faber CG, and Merkies IS. Morphometry of dermal nerve fibers in human skin. *Neurology* 77: 242-249, 2011.
Lenhard, W. and Lenhard, A. Calculation of Effect Sizes. Retrieved from: https://www.psychometrica.de/effect_size.html. Dettelbach (Germany): Psychometrica., 2016.
Lehmann HC, Chen W, Borzan J, Mankowski JL, and Hoke A. Mitochondrial dysfunction in distal axons contributes to human immunodeficiency virus sensory neuropathy. *Annals of neurology* 69: 100-110, 2011.

Marunaka Y. Effects of internal Na and external K concentrations on Na/K coupling of Na,K-pump in frog skeletal muscle. *J Membr Biol* 101: 19-31, 1988.
Nasu S, Misawa S, Nakaseko C, Shibuya K, Isose S, Sekiguchi Y, Mitsuma S, Ohmori S, Iwai Y, Beppu M, Shimizu N, Ohwada C, Takeda Y, Fujimaki Y, and Kuwabara S. Bortezomib-induced neuropathy: axonal membrane depolarization precedes development of neuropathy. *Clin Neurophysiol* 125: 381-387, 2014.
Natera-Naranjo O, Kar AN, Aschrafi A, Gervasi NM, Macgibeny MA, Gioio AE, and Kaplan BB. Local translation of ATP synthase subunit 9 mRNA alters ATP levels and the production of ROS in the axon. *Molecular and Cellular Neuroscience* 49: 263-270, 2012.
Palmgren MG, and Nissen P. P-Type ATPases. *Annual Review of Biophysics* 40: 243-266, 2011.
Pathak D, Shields LY, Mendelsohn BA, Haddad D, Lin W, Gerencser AA, Kim H, Brand MD, Edwards RH, and Nakamura K. The role of mitochondrially derived ATP in synaptic vesicle recycling. *J Biol Chem* 290: 22325-22336, 2015.
Peeling J, Sutherland G, Brown RA, and Curry S. Protective effect of dichloroacetate in a rat model of forebrain ischemia. *Neurosci Lett* 208: 21-24, 1996.
Pellerin L, Pellegri G, Bittar PG, Charnay Y, Bouras C, Martin JL, Stella N, and Magistretti PJ. Evidence supporting the existence of an activity-dependent astrocyte-neuron lactate shuttle. *Dev Neurosci* 20: 291-299, 1998.
Persson AK, Black JA, Gasser A, Cheng X, Fischer TZ, and Waxman SG. Sodium-calcium exchanger and multiple sodium channel isoforms in intra-epidermal nerve terminals. *Mol Pain* 6: 84, 2010.
Persson AK, Hoeijmakers JGJ, Estacion M, Black JA, and Waxman SG. Sodium Channels, Mitochondria, and Axonal Degeneration in Peripheral Neuropathy. *Trends Mol Med* 22: 377-390, 2016.
Persson AK, Kim I, Zhao P, Estacion M, Black JA, and Waxman SG. Sodium channels contribute to degeneration of dorsal root ganglion neurites induced by mitochondrial dysfunction in an in vitro model of axonal injury. *J Neurosci* 33: 19250-19261, 2013a.
Persson AK, Liu S, Faber CG, Merkies IS, Black JA, and Waxman SG. Neuropathy-associated Nav1.7 variant I228M impairs integrity of dorsal root ganglion neuron axons. *Annals of neurology* 73: 140-145, 2013b.
Polydefkis M, Yiannoutsos CT, Cohen BA, Hollander H, Schifitto G, Clifford DB, Simpson DM, Katzenstein D, Shriver S, Hauer P, Brown A, Haidich AB, Moo L, and McArthur JC. Reduced intraepidermal nerve fiber density in HIV-associated sensory neuropathy. *Neurology* 58: 115-119, 2002.
Press C, and Milbrandt J. Nmnat Delays Axonal Degeneration Caused by Mitochondrial and Oxidative Stress. *The Journal of Neuroscience* 28: 4861, 2008.
Rolyan H, Liu S, Hoeijmakers JG, Faber CG, Merkies IS, Lauria G, Black JA, and Waxman SG. A painful neuropathy-associated Nav1.7 mutant leads to time-dependent degeneration of small-diameter axons associated with intracellular Ca2+ dysregulation and decrease in ATP levels. *Mol Pain* 12: 2016.
Rossignol R, Gilkerson R, Aggeler R, Yamagata K, Remington SJ, and Capaldi RA. Energy Substrate Modulates Mitochondrial Structure and Oxidative Capacity in Cancer Cells. *Cancer Research* 64: 985, 2004.
Rueda CB, Llorente-Folch I, Amigo I, Contreras L, González-Sánchez P, Martínez-Valero P, Juaristi I, Pardo B, del Arco A, and Satrústegui J. Ca2+ regulation of mitochondrial function in neurons. *Biochimica et Biophysica Acta (BBA) - Bioenergetics* 1837: 1617-1624, 2014.

Smith AG, Ramachandran P, Tripp S, and Singleton JR. Epidermal nerve innervation in impaired glucose tolerance and diabetes-associated neuropathy. *Neurology* 57: 1701-1704, 2001.
So PW, and Fuller BJ. Enhanced energy metabolism during cold hypoxic organ preservation: studies on rat liver after pyruvate supplementation. *Cryobiology* 46: 295-300, 2003.
Sokoloff L. Energetics of Functional Activation in Neural Tissues. *Neurochemical Research* 24: 321-329, 1999.
Takeuchi H, Mizuno T, Zhang G, Wang J, Kawanokuchi J, Kuno R, and Suzumura A. Neuritic beading induced by activated microglia is an early feature of neuronal dysfunction toward neuronal death by inhibition of mitochondrial respiration and axonal transport. *J Biol Chem* 280: 10444-10454, 2005.
Tanaka T, Nagashima K, Inagaki N, Kioka H, Takashima S, Fukuoka H, Noji H, Kakizuka A, and Imamura H. Glucose-stimulated single pancreatic islets sustain increased cytosolic ATP levels during initial Ca2+ influx and subsequent Ca2+ oscillations. *J Biol Chem* 289: 2205-2216, 2014.
Tanaka Y, Yano H, Ogasawara S, Yoshioka S-i, Imamura H, Okamoto K, and Tsuneoka M. Mild Glucose Starvation Induces KDM2A-Mediated H3K36me2 Demethylation through AMPK To Reduce rRNA Transcription and Cell Proliferation. *Molecular and Cellular Biology* 35: 4170-4184, 2015.
Tantama M, Martinez-Francois JR, Mongeon R, and Yellen G. Imaging energy status in live cells with a fluorescent biosensor of the intracellular ATP-to-ADP ratio. *Nat Commun* 4: 2550, 2013.
Verze L, Paraninfo A, Ramieri G, Viglietti-Panzica C, and Panzica GC. Immunocytochemical evidence of plasticity in the nervous structures of the rat lower lip. *Cell Tissue Res* 297: 203-211, 1999.
Wang P, Chen M, Yang Z, Yu T, Zhu J, Zhou L, Lin J, Fang X, Huang Z, Jiang L, and Tang W. Activation of Pyruvate Dehydrogenase Activity by Dichloroacetate Improves Survival and Neurologic Outcomes After Cardiac Arrest in Rats. *Shock* 49: 704-711, 2018.
Wendt, H. W. Dealing with a common problem in social science: a simplified rank-biserial coefficient of correlation based on the *U* statistic. European Journal of Social Psychology. 2: 463-465, 1972.
Westermann B. Bioenergetic role of mitochondrial fusion and fission. *Biochimica et Biophysica Acta (BBA) - Bioenergetics* 1817: 1833-1838, 2012.
Youle RJ, and van der Bliek AM. Mitochondrial fission, fusion, and stress. *Science (New York, NY)* 337: 1062-1065, 2012.
Zeng J, Yang GY, Ying W, Kelly M, Hirai K, James TL, Swanson RA, and Litt L. Pyruvate improves recovery after PARP-1-associated energy failure induced by oxidative stress in neonatal rat cerebrocortical slices. *J Cereb Blood Flow Metab* 27: 304-315, 2007.

Figure 1. DRG neurons expressing I228M, a gain-of-function mutant of NaV1.7, display reduced neurite length *in vitro*

Mouse DRG neurons were isolated from 6-8 week old mice and sister cultures, prepared at the same time from the same animal by the same operator, were electroporated with the plasmid encoding wild-type Nav1.7 or the mutant channel along with RFP. After the electroporation, cells were plated on the coverslips coated with laminin and cultured for 7 days. The resulting cultures were imaged and their total lengths per cell were assessed as described in Methods.

A. Large-field montage image of WT-expressing DRG culture, consisting of 7X7 field views. Dotted lines distinguish individual field-of-view. Scale bar, 1000μm

B. Enlarged field view image of individual neurons transfected NaV1.7 WT

C. Large-field montage image of I228M-expressing DRG culture, consisting of 7X7 field views. Dotted lines distinguish individual field-of-view. Scale bar, 1000μm

D. Enlarged field view image of individual neurons transfected NaV1.7 I228M

Quantification of total length per cell of WT and I228M neurons calculated from large-field images and the average for each condition. Each data point represents total neurite length per cell from each culture. Dotted line indicates mean value of control. Data are normalized to WT values and presented as mean ± standard deviation. Mean of WT (n = 34 cultures from 8 animals) and I228M (34 cultures from 8 animals) are 1.000 ± 0.1870 and 0.7966 ± 0.1755, respectively. MD (WT - I228M) is 0.2034 ± 0.04398. CI is 0.1155 to 0.2912. I228M culture displays a 20 % decrease in neurite lengths with ****$p < 0.0001$, (nested t test).

Figure 2. DRG neurons expressing I228M display a significant reduction in neurite length at reduced glucose concentrations.

Mouse DRG cultures expressing the indicated channels were prepared as described in Methods. The cultures were then maintained in the culture media containing 25, 5.7, or 2.7mM glucose for 7 days. The resulting cultures were imaged, and their neurite lengths were assessed as described in Methods. Data are normalized to the neurite length values of 25mM glucose cultures and presented as mean ± standard deviation. Dotted line indicates mean value of control.

A. WT neurons show a similar extent of neurite outgrowth in all the range of glucose concentrations (25mM: 1 ± 0.3057, n = 19 cultures from 5 animals ; 5.7mM: 1.1346 ± 0.3452, n = 19 cultures from 5 animals; 2.7mM: 1.1569 ± 0.3740, n = 11 cultures from 3 animals).

B. I228M neurons display neurite length reductions in the low glucose conditions, compared to 25mM glucose (25mM: 1 ± 0.2902, n = 20 cultures from 5 animals; 5.7mM: 0.9036 ± 0.1966, n = 20 cultures from 5 animals; 2.7mM: 0.7471 ± 0.2218 from n = 12 cultures from 3 animals).

I228M-transfected culture displays a 25 % reduction in neurite lengths at 2.7mM glucose, compared to the culture at 25mM glucose (**p = 0.0120, nested one way ANOVA followed by Dunnett's multiple comparisons test. MD (25mM-2.7mM) is 0.2529 ± 0.08847. CI is 0.04879 to 0.4570. In contrast to the mutant culture, WT culture did not show reduced neuritic growths in the low glucose concentrations (NS, not significant, nested one way ANOVA followed by Dunnett's multiple comparisons test).

Figure 3. [ATP]i levels are decreased in DRG neurons expressing I228M.

Steady-state levels of ATP were measured from cultured DRG neurons using a FRET-based ATP indicator approach. ATeam, an ATP FRET probe was expressed in mouse DRG neurons along with the indicated channels. 7 days after culturing, FRET signals of transfected neurons were measured in the absence or the presence of rotenone as described in Methods.

A. Representative FRET images of ATeam-expressing DRG neurons

B. I228M-expressing neurons exhibit a reduced FRET signal, compared to WT neurons (WT: 3.738 ± 0.612 from n = 218 cells; I228M: 3.542 ± 0.770 from n = 121 cells, p = 0.0042, Mann-Whitney test). Each data point represents a FRET value from each cell. Dotted line indicates mean value of control.

C. Representative FRET images of ATeam-expressing DRG neurons treated with rotenone

I228M-expressing neurons exhibit a markedly reduced FRET signal, compared to WT neurons in the presence of rotenone (WT: 3.408 ± 0.800 from n = 250 cells; I228M: 3.031 ± 1.042 from n = 325 cells, p > 0.0001 Mann-Whitney test). Each data point represents a FRET value from each cell. Dotted line indicates mean value of control.

Figure 4. DRG neurons expressing I228M display a rapid ATP reduction, compared to WT neurons in response to membrane depolarization.

ATP kinetics of DRG neurons were assessed in response to depolarization as described in Methods. Mouse DRG neurons transfected with ATeam along with Nav1.7 WT or I228M and FRET changes were monitored after depolarization with 50mM KCl.

A. Representative time-lapse images of ratiometric FRET change of DRG neurons expressing the indicated channels. Scale bar, 50 μm.

B. Traces represent means of WT neurons (n=8) and I228M neurons (n=7). Error bars represent standard deviations.

C. Quantification of FRET changes of DRG neurons after membrane depolarization by 50mM [K+], Area under the curve (AUC) was calculated and the

difference between the groups was analyzed (WT: -222.6±56.2, n=8; I228M: -291.8±25.8, n=7). Dotted line indicates mean value of control.

D. Representative time-lapse images of ratiometric FRET change of DRG neurites expressing the indicated channels. Scale bar, 10 μm.

E. Traces represent means of WT neurites (n=12) and I228M neurites (n=12). Error bars represent standard deviations.

Quantification of FRET changes of DRG neurites after membrane depolarization by 50mM [K+], Area under the curve (AUC) was calculated and the difference between the groups was analyzed (WT: -450.9±169.3, n=12; I228M: -1085±281.2, n=12). Dotted line indicates mean value of control.

Figure 5. Increasing pyruvate availability fails to increase the neurite length of I228M neurons.

I228M neurons were treated as indicated, in order to increase pyruvate availability for mitochondria and assess the effects of those treatments in the neuritic growth. Mouse DRG neurons were isolated from 6-8 weeks old mice and electroporated with the plasmid encoding wild type Nav1.7 or the mutant channel along with RFP. After electroporation, the cells were plated on the coverslips coated with laminin and cultured for 7 days in the indicated treatments.

A. Carbohydrate energy metabolism and its feedback regulation

Using pyruvate, mitochondria produce more ATP through TCA cycle and oxidative phosphorylation (OXPHOS) than glycolysis and lactate fermentation do. Glucose negatively regulate mitochondrial TCA and OXPHOS *via* pyruvate dehydrogenase kinase.

B. The effect of pyruvate supplementation in neurite lengths. Each data point represents total neurite length per cell from each culture. Dotted line indicates mean value of control. Data are normalized to the value of I228M-control (without pyruvate) and presented as mean ± standard deviation (I228M-Control: 1.067 ± 0.413, n = 17 cultures from 6 animals; I228M-pyruvate: 1.284 ± 0.704, n = 15 cultures from 6 animals). Difference between means is not significant (p = 0.2027, nested t test). MD (Control-Pyruvate) is -0.4249 ± 0.3117. CI is -1.120 to 0.2696.

The effect of DCA treatment in neurite lengths. Each data point represents total neurite length per cell from each culture. Dotted line indicates mean value of control. Data are normalized to the value of I228M-control (without DCA treatment) and presented as mean ± standard deviation (I228M-Control: 0.9981 ± 0.301, n = 12 cultures from 3 animals ; I228M-DCA: 1.021 ± 0.387, n = 10 cultures from 3 animals). Difference between means is not significant (p = 0.8827, nested t test). MD (Control-DCA) is -0.02322 ± 0.1551. CI is -0.3490 to 0.3026.

Figure 6. I228M-expressing neurons exhibit alterations in mitochondrial distribution and morphology.

Mitochondria were genetically labeled by transfecting Mito-DsRed into mouse DRG neurons expressing the indicated human Nav1.7 plasmids. Mitochondria with red fluorescence were imaged and counted in transfected neurites, as described in Methods.

A. A representative image of neuritic mitochondria of DRG neurons expressing WT. Scale bar, 50 μm.

B. A representative image of neuritic mitochondria of DRG neurons expressing I228M. Scale bar, 50 μm.

C. Mitochondrial density of WT- and I228M-expressing neurites. Dotted line indicates mean value of control. Each data point represents an individual neurite. Data are normalized to neurite length and presented as mean ± standard deviation. The graph represents mean of mitochondrial numbers per μm. (WT: 0.1449 ± 0.0229, n=39 neurites; I228M: 0.1323 ± 0.0046610298, n=41 neurites, *p = 0.0371, unpaired t test). MD (WT-I228M) is 0.01266 ± 0.005967. CI is -0.02453 to -0.00078.

D. Mitochondrial size of WT- and I228M-expressing neurites. Dotted line indicates mean value of control. Each data point represents an individual mitochondria. Data are presented as mean ± standard deviation. The graph represents the mean of pixel numbers (WT: 112 ± 171.59, n=1453 mitochondria; I228M: 90.47 ± 130.01, n=1014 mitochondria, ***p = 0.007, Mann-Whitney test). I228M neurons display a modest but significant reduction in mitochondrial density and size in neurites, compare to WT neurons.

Figure 7. Dexpramipexole promotes neurite growth of I228M-expressing neurons.

I228M neurons were treated with 2μM dexpramipexole for 7 days and the neurite lengths were compared to those of the untreated group.

A. A representative montaged image of I228M-expressing DRG culture.

B. A field view image of the montaged image shown in A

C. A representative montaged image of I228M-expressing DRG culture in a coverslip.

D. A field view image of the montaged image shown in C

E. Quantification of total length per cell of I228M-control and I228M-treatment group. Dotted line indicates mean value of control. Each data point represents total neurite length per cell from each culture. Data are normalized to neurite control value and presented as mean ± standard deviation (I228M-Control: 1 ± 0.0974, n = 12 cultures from 3 animals; I228M-2μM dexpramipexole: 1.287 ± 0.08403, n = 12 cultures from 3 animals). MD (DEX-Control) is 0.2875 ± 0.09296. CI is -0.009469 to

0.4803. Dex-treated I228M culture displays a 29 % increase in neurite lengths with ***p = 0.0053, (nested t test).

F. Quantification of total length per cell of WT-control and WT-treatment group. Dotted line indicates mean value of control. Each data point represents total neurite length per cell from each culture. Data are normalized to neurite control value and presented as mean ± standard deviation (WT-Control: 1 ± 0.0828 from n = 10 cultures from 3 animals; WT-2μM dexpramipexole: 1.034 ± 0.0839, n = 10 cultures from 3 animals). MD (DEX-Control) is -0.03392 ± 0.1179. CI is -0.2816 to 0.2138. Dex-treated WT culture did not displays any significant change in neurite lengths. (p = 0.7768, Nested t test).

Figure 1, Lee *et al.*

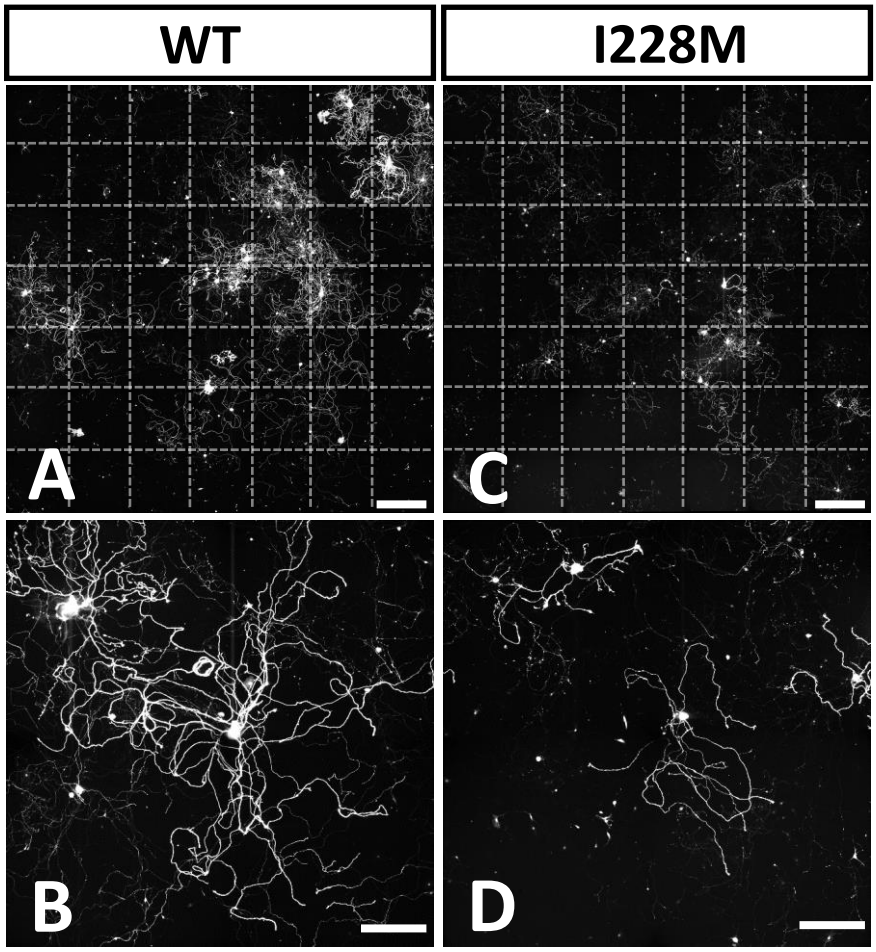

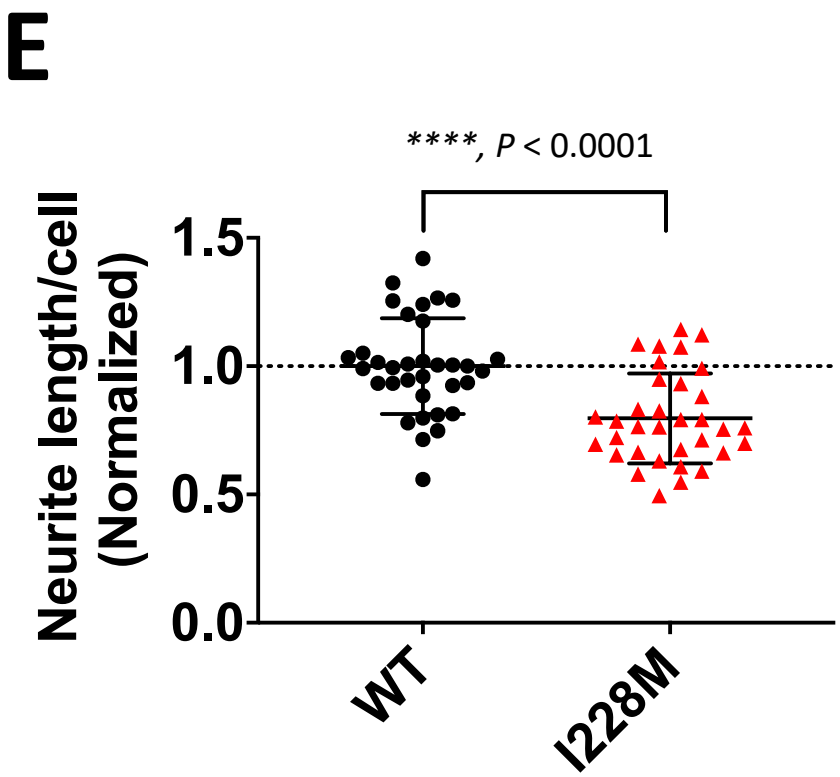

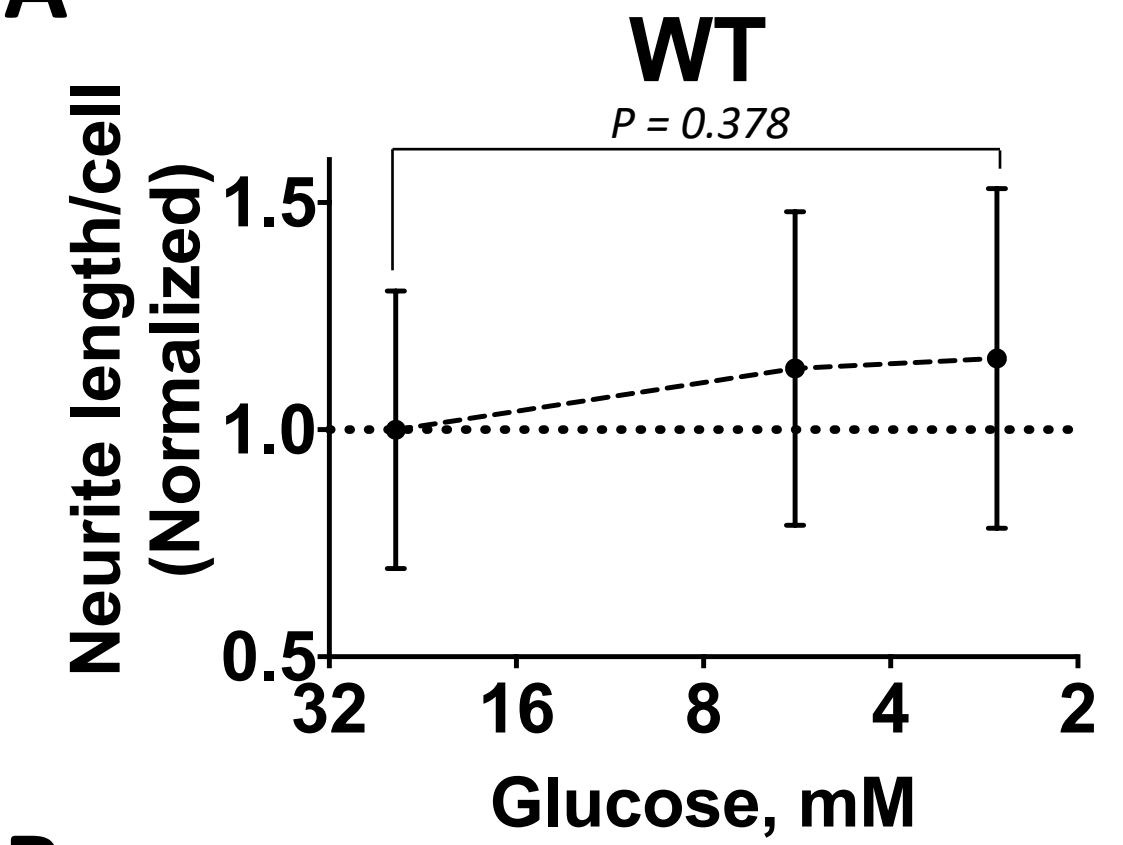

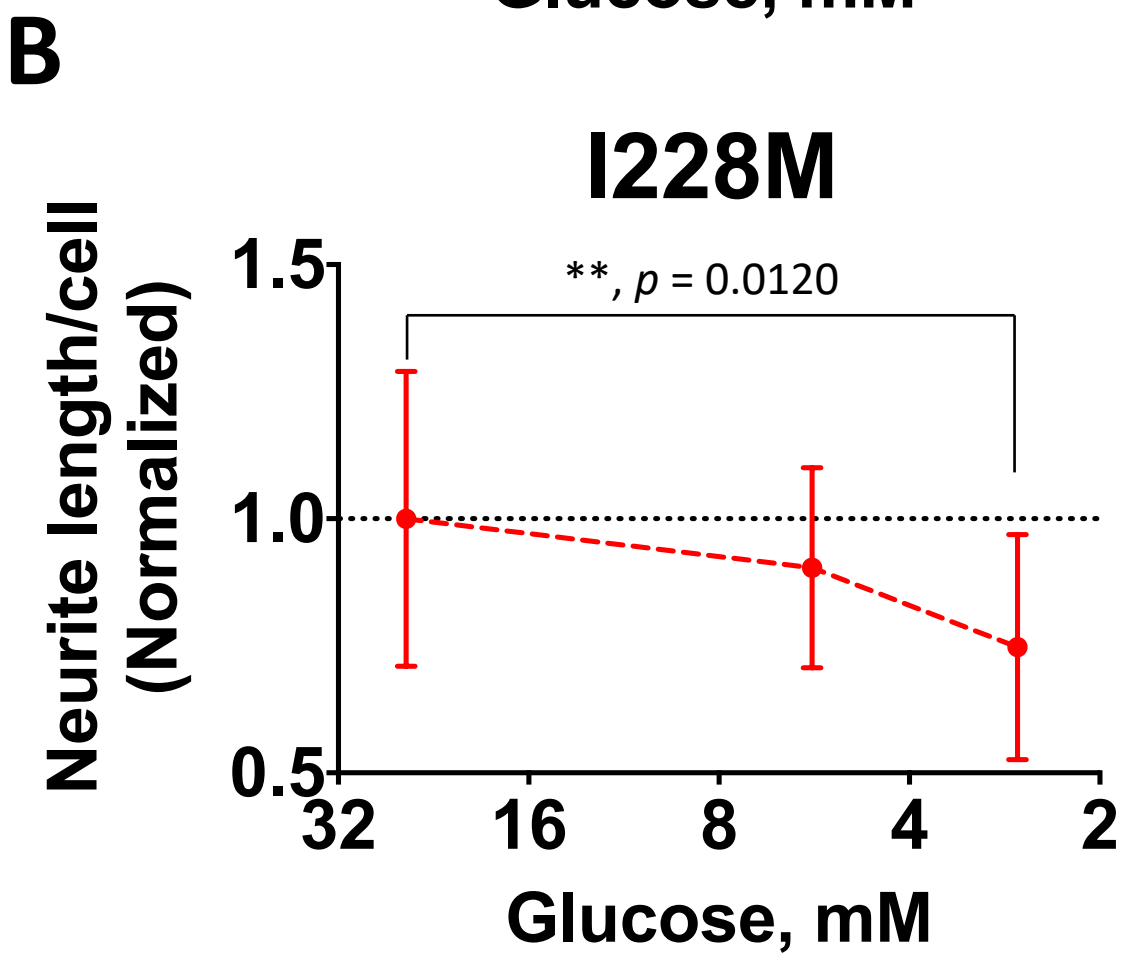

Figure 3, Lee *et al.*

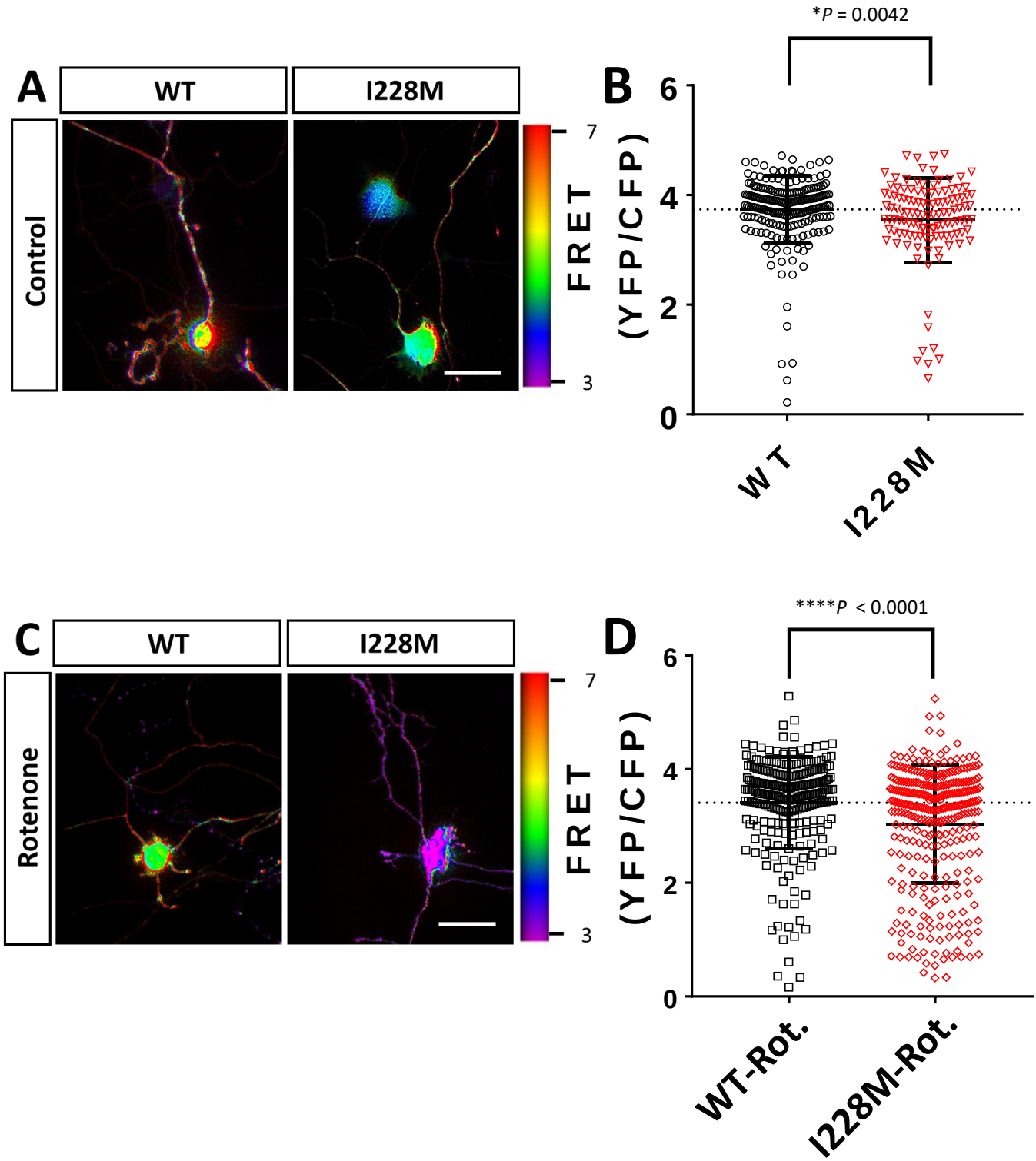

Figure 4, Lee *et al.*

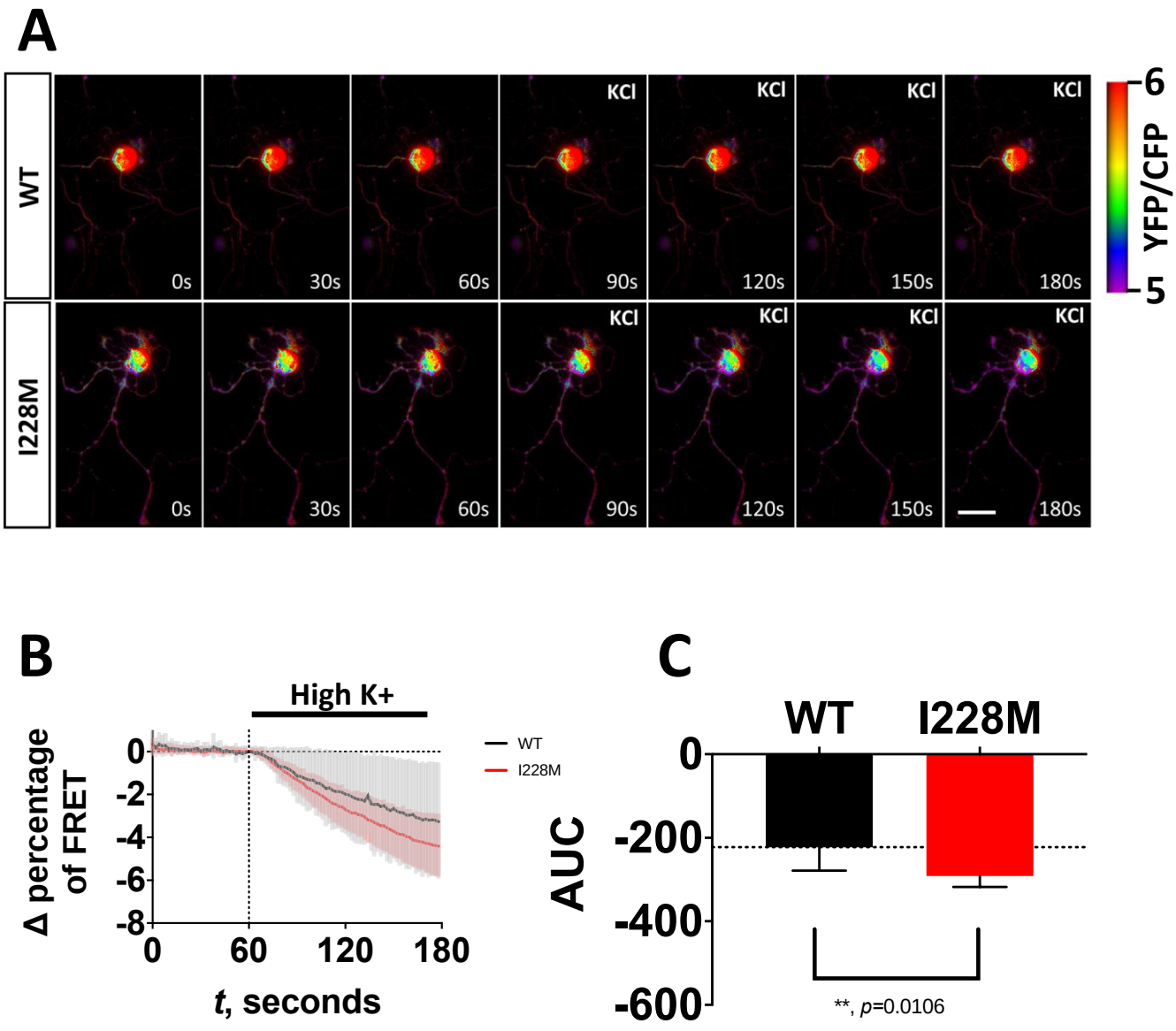

Figure 4, Lee *et al.*

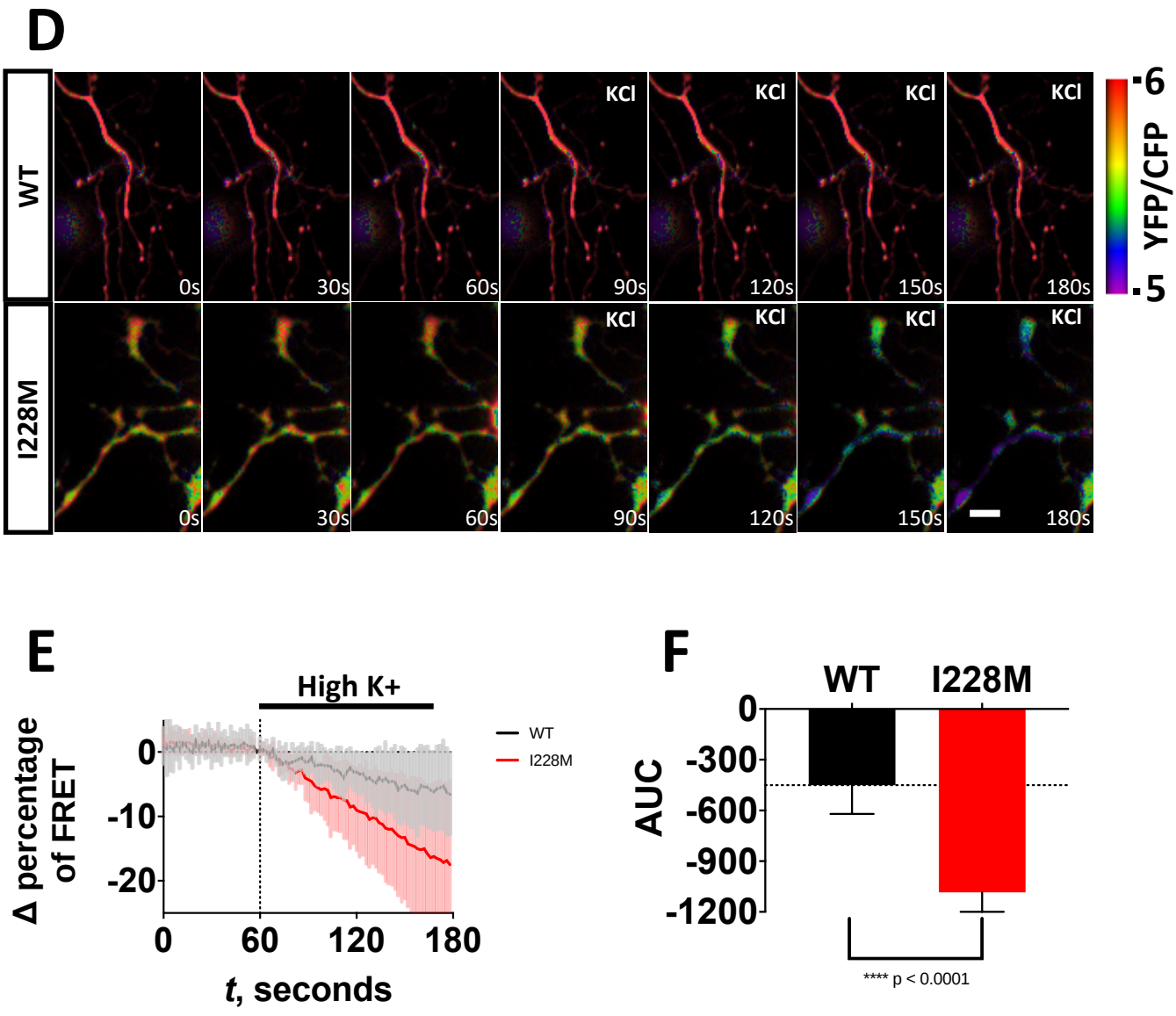

Figure 5, Lee *et al.*

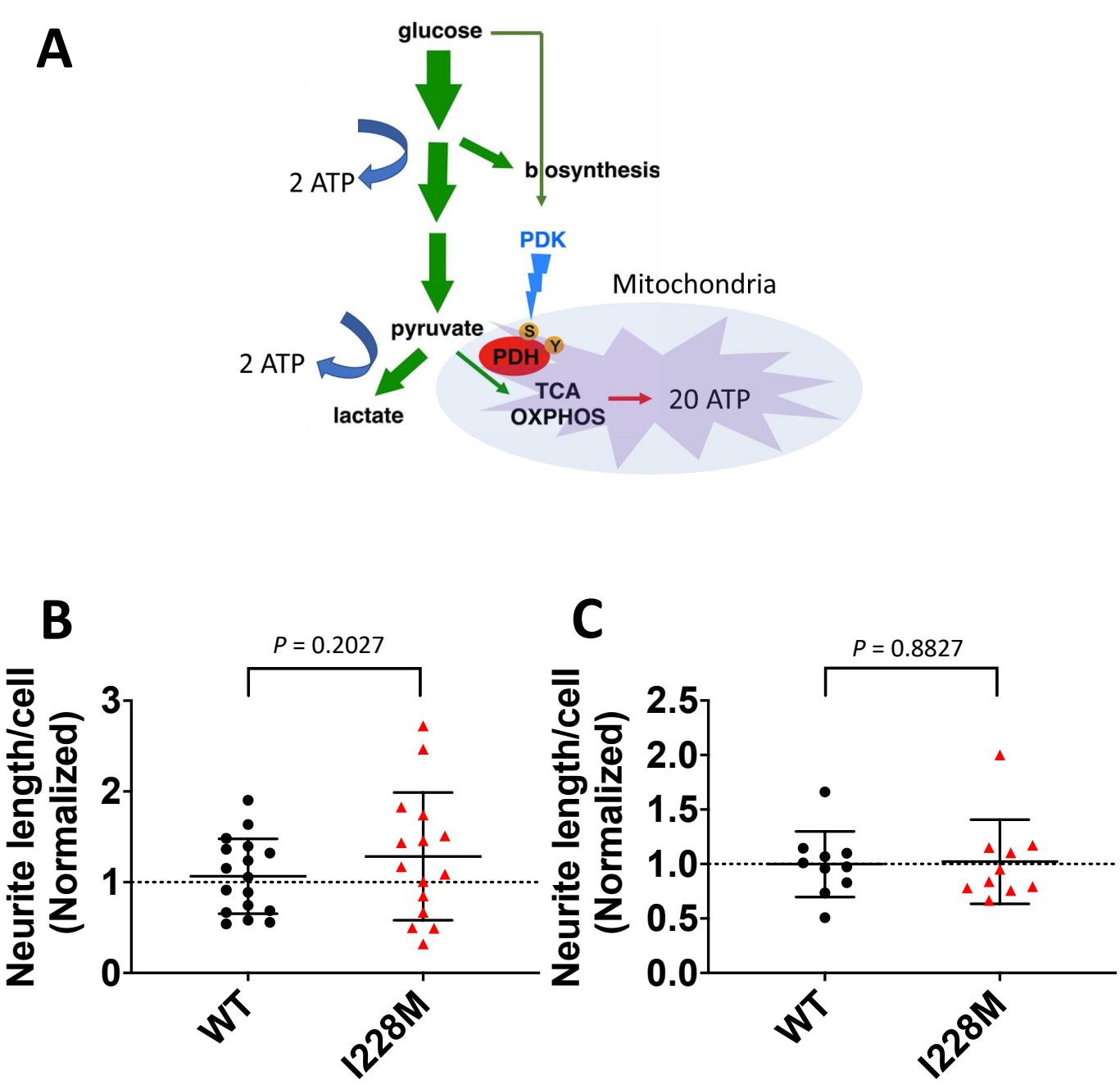

Figure 6, Lee *et al.*